Honeycomb-like PLGA-*b*-PEG Structure Creation with T-junction Micro Droplets

Merve Gultekinoglu[1,2]‡, Xinyue Jiang[3]‡, Cem Bayram[4], Kezban Ulubayram[1,2,5,6], Mohan Edirisinghe[3]*

[1]Department of Basic Pharmaceutical Sciences, Faculty of Pharmacy, Hacettepe University, Turkey

[2]Bioengineering Division, Institute for Graduate Studies in Science & Engineering, Hacettepe University, Turkey

[3]Department of Mechanical Engineering, University College London (UCL), London WC1E 7JE, UK

[4]Advanced Technologies Application and Research Center, Hacettepe University, Ankara, Turkey

[5]Nanotechnology and Nanomedicine Division, Institute for Graduate Studies in Science & Engineering, Hacettepe University, Turkey

[6]Polymer Science and Technology Division, Institute for Graduate Studies in Science & Engineering, Hacettepe University, Turkey

‡ MG and XJ contributed equally to this work.

* Corresponding author ME- m.edirisinghe@ucl.ac.uk

ABSTRACT

Amphiphilic block copolymers are widely used in science owing to their versatile properties. In this study, amphiphilic block copolymer poly(lactic-co-glycolic acid)-block-poly(ethylene glycol) (PLGA-*b*-PEG) was used to create micro droplets in a T-junction microfluidic device with a well-defined geometry. In order to compare interfacial characteristics of micro droplets, dichloromethane (DCM) and chloroform were used to prepare PLGA-*b*-PEG solution as an oil phase. In the T-junction device water and oil phases were manipulated at variable flow rates from 50 µL/min to 300 µL/min by increments of 50 µL/min. Fabricated micro droplets were directly collected on a glass slide. After a drying period, porous 2D and 3D structures were obtained as honeycomb-like structure. Pore sizes were increased according to increased water/oil flow rate for both DCM and chloroform solutions. Also it was shown that increasing polymer concentration decreased the pore size of honeycomb-like structures at a constant water/oil flow rate (50/50 µL/min). Additionally, PLGA-*b*-PEG nanoparticles were also obtained on the struts of honeycomb-like structures according to the water solubility, volatility and viscosity properties of oil phases, by the aid of Marangoni flow. The resulting structures has a great potential to be used in biomedical applications, especially in drug delivery related studies with nanoparticle forming ability and cellular responses in different surface morphologies.

KEYWORDS: PLGA-*b*-PEG; microfluidic; T-junction; honeycomb; Marangoni.

1. INTRODUCTION

Porous polymeric structures as an extracellular matrix (ECM) analogue provide a spatial conformation and orientation to cells and permits nutrient transport, fulfilling a pivotal role in tissue engineering[1-2]. The control of porosity and pore shape is crucial for the polymeric membranes and scaffolds since the size of the pores directs the cell and nutrition transport through the scaffold[3]. Cell viability, proliferation, differentiation, gene expression and migration properties are directly influenced by the physical properties of the pores in terms of size, porosity and inter-pore connectivity[4]. Moreover, the uniformity of the pores strongly affects the mechanical properties and irregularity of pore size and geometries results an inhomogeneous reaction throughout the polymeric structures. Amongst the aforementioned disciplines materials science and engineering mostly focuses on the scaffold design and fabrication steps which is the key step for the fate of the cells to be cultured. Several conventional methods have been proposed to construct porous membranes and scaffolds such as freeze-drying, gas forming, particulate leaching or electrospinning[5-7]. However, both uniform pore size distribution and well-defined pore geometry, as well as interconnection between the pores cannot precisely be generated or requires multiple steps.

Synthesis of polymeric vesicles via conventional emulsion systems dates back to decades ago; however, microfluidic systems featured studies have become widespread recently[8-10]. The first and foremost advantage of the microfluidics derived polymeric micro droplets is the monodispersity, and also the size of these homogenous droplets can be finely tuned by adjusting the fluid flow rates[11-12]. Apart from obtaining individual spherical

polymeric particles through microfluidic systems, these finely tuned droplets in emulsion systems can be further utilized for 2D and 3D material production[13]. Ordered porous films and porous scaffolds to be used as biomaterials for tissue engineering applications can be fabricated via microfluidic systems for the collection of monosized microbubbles. Fabrication of porous structures via microfluidic devices has many important advantages, such as not requiring a template for removal step, precise control of pore size and reproducibility, most of which cannot be achieved in single step conventional methods. Although some newly introduced techniques such as stereolithography, direct 3D writing have been recently reported for the fabricating well-ordered and highly uniform structures, these techniques are costly examples both with respect to time and resources. Microfluidic production of ordered porous structures can resolve the major drawbacks of conventional fabrication of aforesaid structures, such as pore size distribution, multi-step preparation and irregular geometries of pores, which are all application limiting issues[14].

Recently, a one-step porous film fabrication was proposed by Elsayed et al., via controlled bursting of monodispersed nitrogen trapped alginate microbubbles[3]. Here they produced alginate sheathed microbubbles through a T-junction type microfluidic device and collected the product on a glass slide. The resultant polymeric porous film was found to be homogenous, controllable in pore size and scalable as well. In a different study conducted by Chung et al.[15], three dimensional alginate scaffolds were produced in a microfluidic flow focusing device after collecting into a vessel containing concentrated calcium chloride as a crosslinking solution. The resulting structure expressed superior properties compared with conventional alginate scaffolds and pore sizes were found to be controllable by adjusting gas pressure, flow rate and viscosity as well. Colosi et al.[16]

obtained an interpenetrating three dimensional network structure using poly (vinyl alcohol) after crosslinking the microbubble structures with glutaraldehyde. New structures were reported to have better porosity with respect to ones fabricated via conventional gas foaming after the evaluation by Scanning Electron Microscopy (SEM) and Micro Computational Tomography (m-CT) images. Several additional examples for microfluidic fabrication with various biocompatible polymers regarding flow focusing and subsequent crosslinking of produced droplet can be found in the literature e.g. gelatine, gelatine methacrylate (GelMA)[17-18]. Wang et al.[4] reported that gelatine honeycomb-like scaffolds have been produced with flow focusing in a microfluidic device, and these highly dimensioned porous structures have demonstrated superior cell viability, proliferation and glycosaminoglycan production as opposed to traditionally freeze-dried porous gelatine skeletons for cartilage regeneration. In addition, it has been reported that accordion-like honeycomb polyglycerol sebacate scaffolds which have been fabricated by microablating, have overcome structural and mechanical limitations of myocardial tissue engineering[19]. Additionally, Eniwumide et al[20], stated that honeycomb-like surfaces may be useful to control the fate of chondrocytes, since being naturally round, these may have been adversely affected by conventional flat surfaces. Consequently, it is possible to fabricate porous scaffolds having a known and well-defined dimensions with a T-junction microfluidic device. Also, this technique is simple and fast and do not require a template and complex set up.

In this study, we aim to fabricate highly oriented porous PLGA-*b*-PEG 2D membranes and 3D scaffolds with a well-defined geometry by using a T-junction microfluidic device. Stereolithograpy, 3D printers, microablation technologies have been widely used to

fabricate scaffolds with a well-defined geometry but the main disadvantages of these techniques are poor cost effectiveness and complicated procedures. On the other hand, microfluidic technology makes it possible to produce scaffolds by one step with very low cost[21-22]. Therefore, we investigated micro-droplet formation in the T-junction channel and collected the resulting products on a glass slide at the end of the tip, directly. During the study PLGA-*b*-PEG honeycomb-like porous structures were fabricated by a one-step approach via a microfluidics device using a single T-junction and formation mechanisms were discussed in terms of solvent type, collection method, polymer concentration and flow intensities. We used dichloromethane (DCM) and chloroform because of the slight miscibility with water and therefore micro droplets were obtained. Poly (lactic-co-glycolic acid)-poly ethylene glycol (PLGA-*b*-PEG) diblock copolymer was used as the polymeric material, since it is widely used in biomaterials research because of its biocompatible and biodegradable properties[23-25]. In addition, once the porous PLGA-*b*-PEG construct is obtained, it preserves its structural integrity without any need for second crosslinking step. Resulting porous polymer structures have great potential as biomaterials for used as tissue scaffolds, implant coatings, patches/dressings with drug delivery features.

2. MATERIALS AND METHODS

2.1. Materials and Preparation of Polymeric Solutions

Poly(lactic-co-glycolic acid)-block-Poly(ethylene glycol) (PLGA-*b*-PEG, 50:50), Resomer RGP d50105 (Mw=50000 g/mol) (diblock, 10% PEG with 5000 Dalton) was purchased from Boehringer Ingelheim Pharma GmbH&Co Ingelheim, Germany. Chloroform HPLC grade ≥99.9 %, Dichloromethane (DCM) HPLC grade ≥99.9% and Nile Red dye (for microscopy) were obtained from Sigma-Aldrich, Germany and used directly. T-junction

setup was fabricated with Polydimethylsiloxane (PDMS) by CNC machine, in the University College London (UCL) Mechanical Engineering workshop, UK.

Polymeric solutions of PLGA-*b*-PEG was prepared in either DCM or chloroform and stirred 2 hours prior to usage. PLGA-*b*-PEG was dissolved at 2.5, 5 and 10 % (w/v) concentrations in DCM and chloroform.

2.2. Solution Characterizations

PLGA-*b*-PEG solution properties were investigated for each concentration. Surface tension parameters were determined by a Kruss tensiometer (model K9, Kruss GmbH, Germany). Viscosity parameters of the polymeric solution were measured with a U-tube viscometer (Ostwald viscometer) and calculated with Equation 1.

$$\eta_{rel} = \frac{\eta}{\eta_0} = \frac{\rho\, t}{\rho_0\, t_0} \qquad (1)$$

Where η_{rel} is the relative viscosity, ρ is the sample solution density, t is the time of outflow of the sample solution, ρ_0 is the blank solution (water) density, t_0 is the time of outflow of the blank solution (water), η_0 is the viscosity of water and then η is calculated through the Equation 1. Equipment was calibrated prior to usage and all the measurements were performed at ambient conditions (~ 20 °C, % relative humidity 42).

2.3. Micro droplet Fabrication with T-junction Microfluidic Device

An illustration of the microfluidic T-junction device used in this work is shown in Figure 1. This T-junction was made by perpendicularly inserting two Teflon FEP (Fluorinated Ethylene Polypropylene) capillary tubing with inner diameter of 200 μm into a

Polydimethylsiloxane (PDMS) block as inlet channels for the two immiscible liquid flows. A third capillary of 200 μm inner diameter was screwed into the exit channel of the block. The intersectional gap area of 200 μm was created by aligning the polymeric solution inlet and exit channels, and this resulted in a confluence junction of two immiscible phases. Both liquid inlets were supplied by syringe pumps (Harvard Apparatus Ltd., Edenbridge UK). All capillaries were fixed and secured to the channels by connectors to prevent leakage of liquid. Micro droplets were obtained using glass slides from the end of exit capillary of the microfluidic T-junction as shown in Figure 1. Later, optical microscopy was used to observe the structure of micro droplet and honeycomb-like structures. Honeycomb-like structures were produced after drying out micro droplets obtained on glass slides.

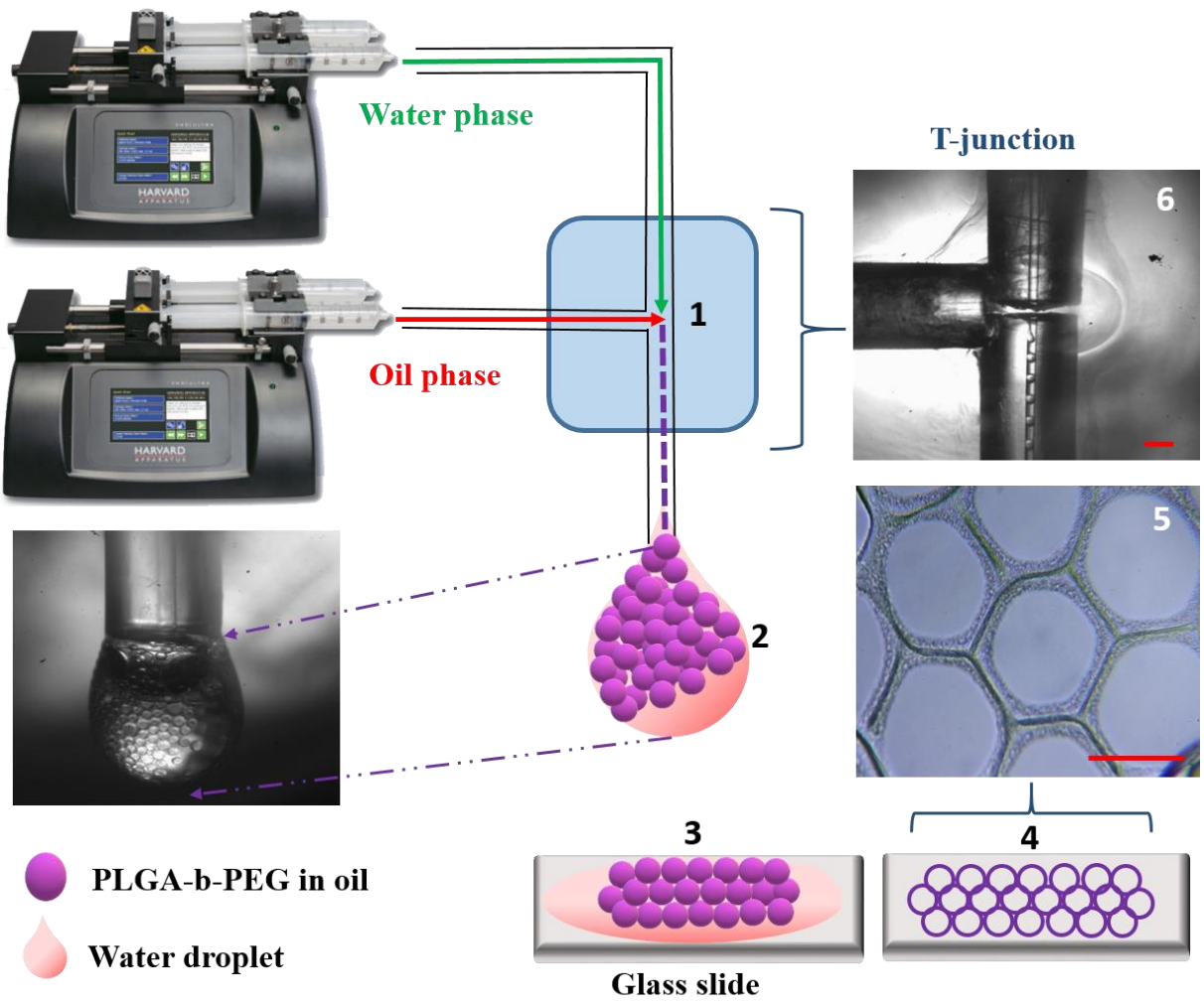

Figure 1. Schematic representations of micro droplet fabrication with T-junction microfluidic device set-up (1-2) (inset shows the tip end of the junction), collected layer on the top of glass slide (3) and honeycomb-like structure production (4). The optical microscope image of the honeycomb-like structure, scale bar=100μm (5). High-speed camera frame of T-junction module, scale bar=500μm (6).

A phantom 7.3 high speed camera with a maximum resolution of 800 * 600 pixels at up to 4800 fps giving recording duration of 1.2 seconds (Vision Research Ltd., UK) was utilized to record the formation of the micro droplets inside the T-junction channel and at the tip end with real time video images.

2.4. Characterization of 2D and 3D Honeycomb-like Structures

2D and 3D PLGA-*b*-PEG structures were morphologically examined by Optical Light Microscopy (Zeiss Axiotech, Germany) fitted with a camera (Nikon Eclipse ME 600, Japan) and Scanning Electron Microscopy (SEM, Hitachi S3400, Japan). All the samples were coated with a thin gold layer prior to SEM analysis (Edwards sputter coater). In addition, the sample solutions of PLGA-*b*-PEG with % 5 (w/v) concentration were mixed with Nile Red dye and obtained honeycomb-like structures were examined with Fluorescence Microscopy (EVOS FL Cell Imaging System, Invitrogen, USA). The pore size of the PLGA-*b*-PEG honeycomb-like structures were determined using Image J software program (version 2.71).

3. RESULTS AND DISCUSSION

3.1. Solution Properties of PLGA-*b*-PEG Oil Phase

Solution properties, especially surface tension and viscosity, are the major dominant factors in microfluidic systems and known to effect micro droplet forming directly. Table 1 summarizes the properties of used solutions during the experimental procedures. Viscosity of the PLGA-*b*-PEG was found to be increasing with concentration of the solution; however high viscosity at 10% concentration of both solvents did not cause any problem and homogenous micro droplets were generated. Surface tension decreased at elevated concentrations in both solvents. Additionally, surface tension values of PLGA-*b*-PEG were found higher in chloroform when the concentration was kept constant, since the surface tension of chloroform itself is higher than DCM at ambient temperature.

Table 1. Solution properties of PLGA-*b*-PEG in terms of solvent, concentration, surface tension and viscosity.

Solution	Polymer	Solvent	Concentration % (w/v)	Surface tension (mN/m)	Viscosity (mPa s)
1	PLGA-*b*-PEG	DCM	10	10,8	13,2
2	PLGA-*b*-PEG	DCM	5	10,9	1,3
3	PLGA-*b*-PEG	DCM	2.5	11	0,8
4	PLGA-*b*-PEG	Chloroform	10	10,9	24
5	PLGA-*b*-PEG	Chloroform	5	11,2	4,9
6	PLGA-*b*-PEG	Chloroform	2.5	11,2	1,2

3.2. Micro droplet Formation and Collection to Assemble Honeycomb-like Structures

In this work, the PLGA-*b*-PEG solution is fed at a constant flow rate provided by the syringe pump for the formation of micro droplets. The micro droplet generation process begins when the dispersed phase reaches the cross-sectional gap area of the T-junction, enters the continuous phase and droplet formation starts. There are three main micro droplet formation regimes: dripping, squeezing and jetting[26-27]. Capillary number (Ca) is the physical parameter which dominates micro droplet formation regimes. Capillary number is the ratio of viscous force and surface tension of the interface between two immiscible liquids. Capillary number is calculated using Equation 2 where, Ca is capillary number, η is liquid viscosity, u is droplet front velocity and γ is the surface tension[28].

$$Ca = \eta u/\gamma \qquad (2)$$

In the dripping regime, droplet generation happens when the viscous shear stress overcomes the interfacial tension. If Ca is large enough, the micro droplets are jetted before their size can actually obstruct the channel. Thus, if Ca is small enough, the emerging micro droplet will obstruct the channel and therefore restrict the continuous phase[29]. This will lead to a dramatic hydrodynamic pressure increase in the upstream side of the micro droplets, which results in the pinch-off of the micro droplets. There are so-called separate jetting and squeezing regimes. The diameter of the micro droplet can be manipulated by varying the ratio of liquid flow rate, polymer solution physical parameters (viscosity, surface tension, concentration), and the channel dimension. For a solution with fixed viscosity and flow rate, monodisperse micro droplet generation only occurs in a certain range of the provided liquid flow rate.

In this study, micro droplet generation happened passively. Owing to the small Ca value (0.003) in our experiments, the formation process is found to be in the squeezing regimes. According to the supplementary information of micro droplet formation Video 1 (supplementary information 1-SI1), the front tip of the dispersed phase liquid entered into the main channel and a pressure drop formed between the upstream and downstream of the forming droplet. At the neck of the T-junction, the upstream stress was weakened by interfacial tension and shear stress to form micro droplets from the dispersed phase. Then micro droplets were generated. By varying the liquid flow rate, viscosity, surface tension and concentration of the two immiscible solutions, different size ranges of monodispersed micro droplets can be generated.

Micro droplets obtained from the outlet of the T-junction (SI2) on the microscope glass slides were examined under an optical microscope. Mono dispersed droplets aligned in

an ordered pattern in 2D environment, which later on lead to porous honeycomb-like structures post bursting. The formation of porous honeycomb-like structures occurs in the aqueous phase by polymer diffusion (oil phase droplets). After the oil droplets exploded and dried, the PLGA-*b*-PEG amphiphilic polymer was precipitated in the aqueous medium as a honeycomb-like structure according to the circular spread of micro droplets. Figure 2 shows the schematic formation mechanism of porous honeycomb-like structures from PLGA-*b*-PEG containing perfectly organized monodispersed micro droplets. Here, volatile oil phase, either chloroform or DCM, starts to evaporate in w/o emulsion in this confined dimensions and the interaction of PEG ends with dispersion phase increases at the oil-water junction, subsequently rupture of polymeric sheath occurs. The resulting honeycomb-like membrane structure after drying consists of a PLGA-*b*-PEG pattern with uniform pore sizes. The parameters affecting the pore shape and size will be discussed in sections 3.3. and 3.4. Figure 3 shows the representative images of obtained porous honeycomb-like structures after drying. Both porous membranes and scaffold-like 3D structures were produced after drying micro droplets obtained on substrates depending on the collection type. 2D structures were collected as monolayer while 3D ones in multilayers on glass slides. Uniform 3D structure consisting micro-droplets are formed by up to 2-3 layers on glass slides, due to slip from top of one another. However, if the droplets are collected in confined volumes it is possible to collect multilayer scaffold like structures. In this paper, we focused on the production and characterization of the structures. In figure 3, representative multi-layered examples were shown to point out the possibility of obtaining such structures and it is possible to obtain in both DCM and chloroform.

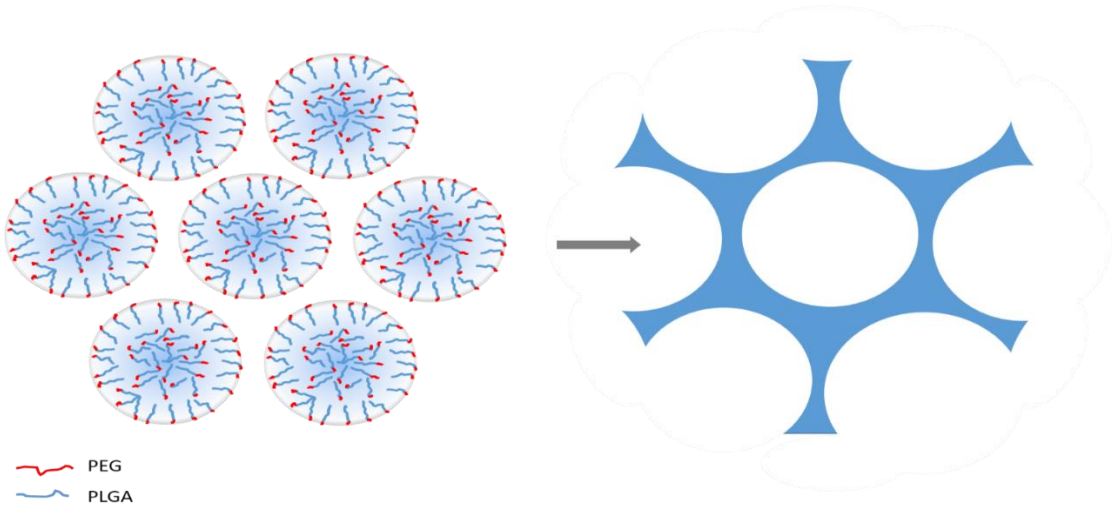

Figure 2. Schematic representation of PLGA-*b*-PEG micro droplets with the chain orientation of hydrophobic and hydrophilic counterparts (left) and honeycomb-like structures which occur after bursting and drying steps (right).

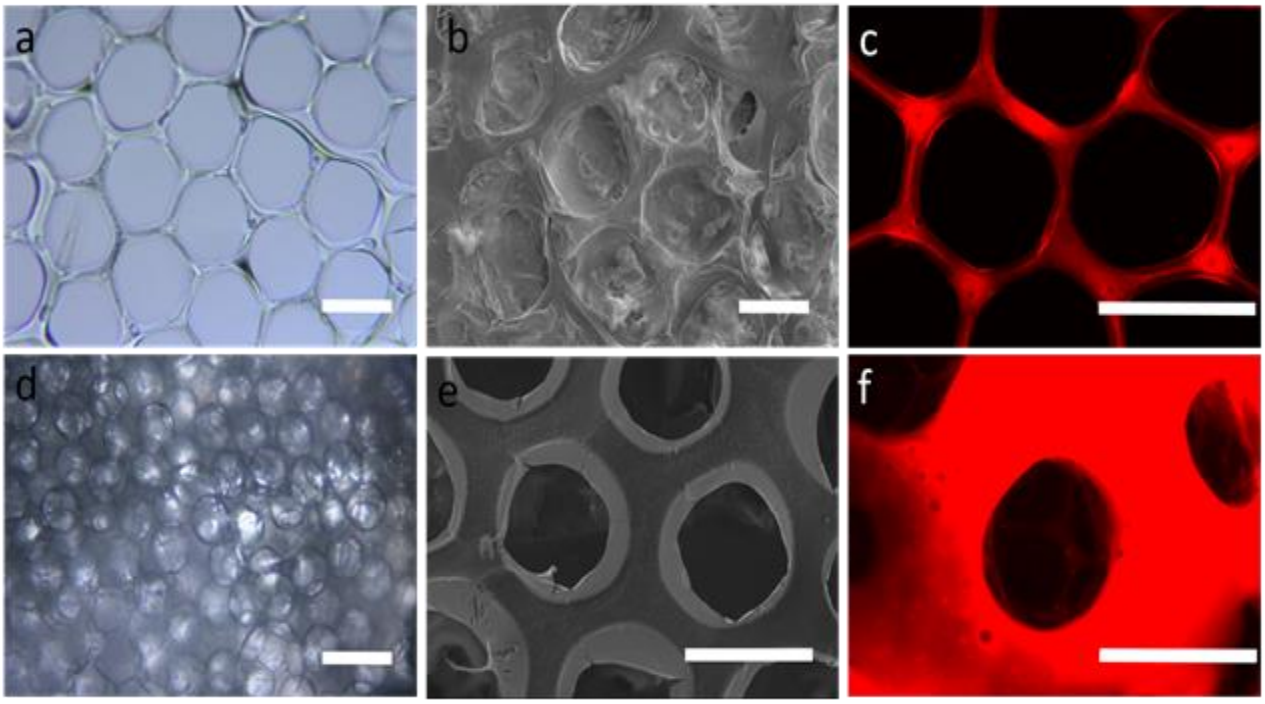

Figure 3. 2D (a-c) and 3D (d-f) honeycomb-like structures produced. Micrographs were taken with optical (a,d), scanning electron (b,e) and fluorescent microscope (stained with Nile Red) (c,f). The concentration of PLGA-*b*-PEG is 5% in DCM and the water/oil flow rate was 1 in all samples. Scale bars indicate 100 μm (a,b,d,e) 200 μm (c) and 400 μm (f).

3.3. Effect of Flow Rate on Porous Structures

In a typical liquid-liquid fluidics process in T-junction geometries, two immiscible fluids form an interface and the penetration of discontinuous phase into the main channel generates the “droplet”[30]. As the droplet grows in the neck, the pressure applied by the continuous flow pushes the penetrated liquid extension downstream and the droplet breaks. The process repeats itself after the tip of the discontinuous phase retracts to the junction and penetrates again[31]. The volume of the droplet can be adjusted by the flow rates of both carrier and dispersion phases. Here, water phase (dispersion) / oil phase (carrier) (w/o) flow rate was chosen as the first parameter for the evaluation of porous structures. Then, PLGA-*b*-PEG concentration was kept constant at 10 % w/w during this investigation. Both DCM and chloroform were tested as organic phase during the investigation.

At a constant flow rate of 100 µL/min for the oil phase, water phase flow was increased from 50 µL/min to 300 µL/min by increments of 50 µL/min. The average droplet size was found to be increasing as the water/oil flow rate increased. The increase was observed in both solvent, however droplet formation could not be observed when the water/oil flow rate above 2 for chloroform. At water/oil flow rates of 2.5 and 3, necking part of discontinuous phase extends without a break-up of droplet, since oil phase cannot penetrate enough to be exposed to the shear stress exerted by the water phase, so the evaluation of flow rates on porous structures was investigated only between 0.5 and 2 with chloroform. According to the shearing model in T-junction droplet forming, at high water flow rates the applied shear stress on the droplet at the end of the neck decrease because of the increasing difference of the speeds of two phases. On the other hand, this

case was not observed when DCM was used as discontinuous phase. This situation can be explained based on the viscosity difference between two solutions as can be seen in Table 1. Viscosities were measured for 10% PLGA-*b*-PEG in both DCM and chloroform as 13.2 and 24 mPa s, respectively. Table 2 summarizes the pore size values of the 2D honeycomb-like structures after drying. Pore sizes directly related with the volume of the droplets broken up through the stream as can be seen in Figures 4 and 5. The diameters of the pores were ranging between 84 to 165 μm with less than 8% deviation from the average, as the water/oil flow rate range was 0.5 to 2.5 when DCM used as solvent. The increase in diameters was also observed at 300 μL/min water flow rate, however in this case deviation was calculated as 13%, which brought an irregularity in pore shapes and orientations as a result of the high diameter differences in droplet size, which can be seen in Figure 4f. Same increasing trend and uniformity in pore shapes were observed in chloroform samples. Average pore diameters were found between 76 to 151 μm with less than 7% deviation at all flow rate because of monodispersed droplet formation. In addition, statistical analysis was carried out according to the pore size calculations. Pore sizes for each flow rate assayed were found as statistically not different using DCM and $CHCl_3$ ($p > 0,05$). However, the increase in pore sizes at flow rate increments between 0.5 to 1, 1 to 1.5, 2 to 2.5 and 2.5 to 3 were found statistically different for DCM and 0.5 to 1 and 1.5 to 2 for $CHCl_3$ ($p < 0,05$).

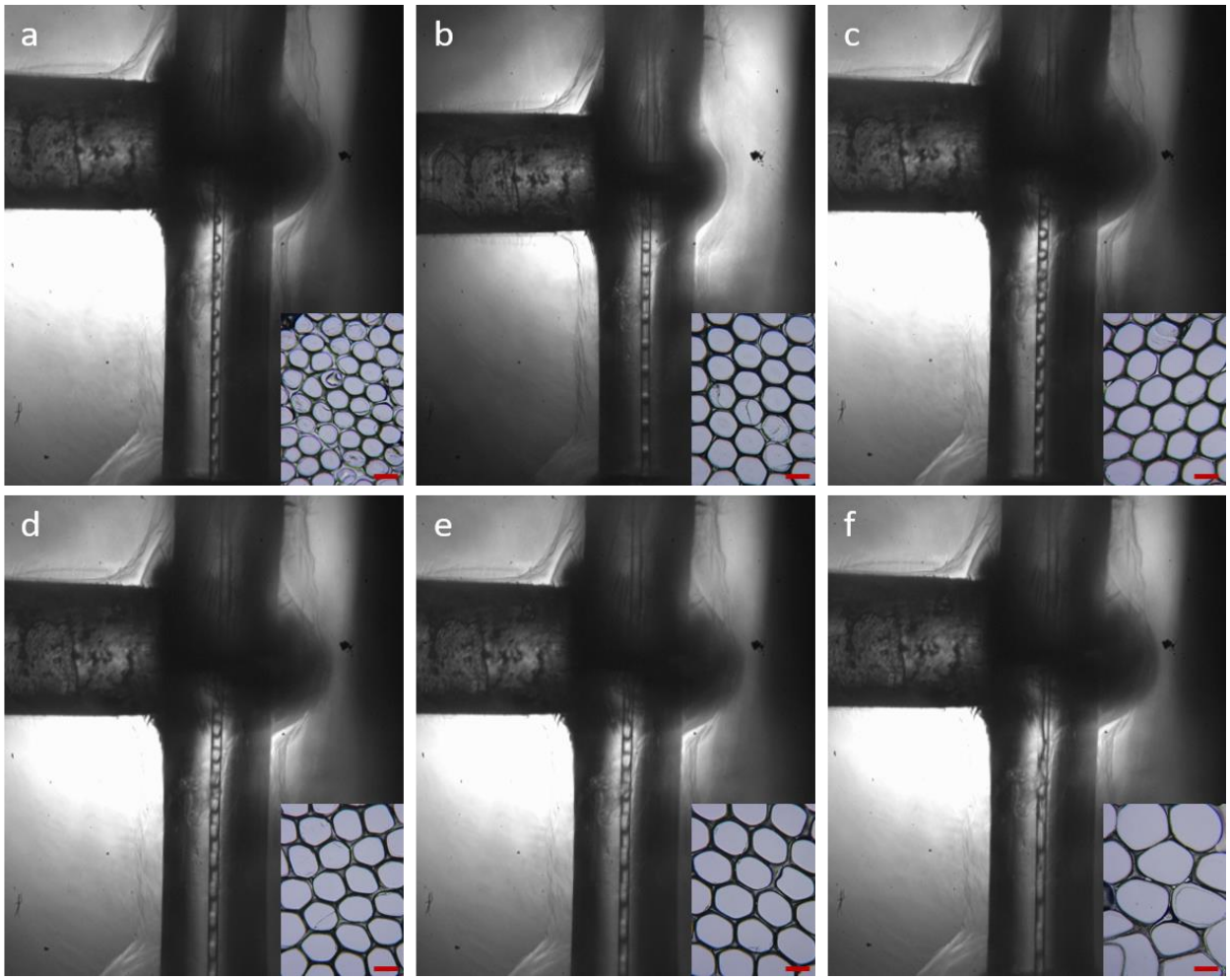

Figure 4. Effect of flow ratio on shapes and pore sizes of honeycomb-like structures formed using DCM. Flow rates (water/oil) are 0.5, 1, 1.5, 2, 2.5 and 3 for a to f, respectively. (Inset scale bars=100 μm)

Table 2. Effect of flow rate on pore size of honeycomb-like structures produced with % 10 (w/v) PLGA-*b*-PEG solution (N/A=not applicable).

		Flow rate (water/oil)					
	Solvent	0.5	1	1.5	2	2.5	3
Pore size (μm)	DCM	84±6	124±4	141±6	147±10	165±8	212±27
	Chloroform	76±3	129±6	134±5	151±10	N/A	N/A

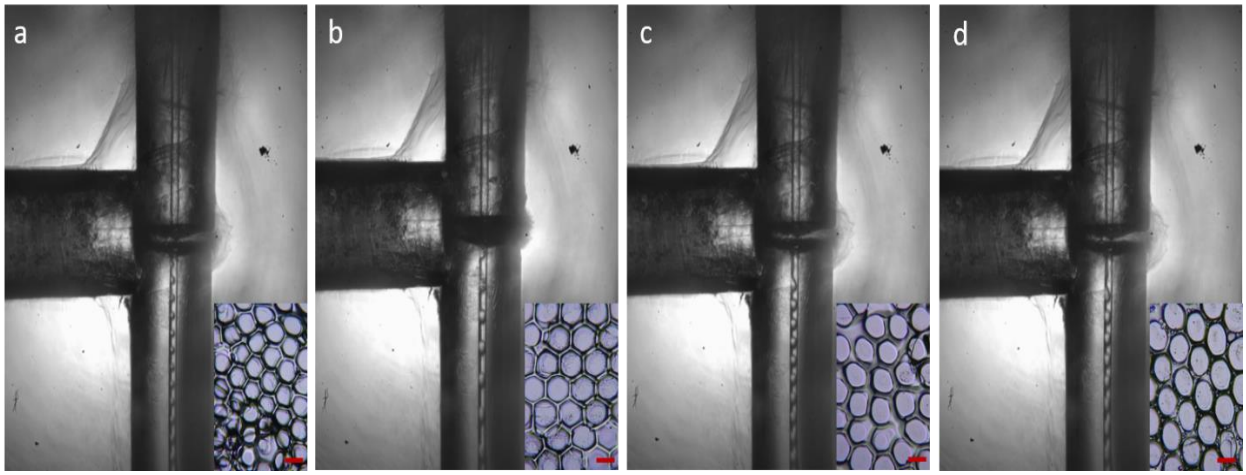

Figure 5. Effect of flow ratio on shapes and pore sizes of honeycomb-like structures formed using chloroform ($CHCl_3$). Flow rates (water/oil) are 0.5, 1, 1.5 and 2 for a to d, respectively. (Inset scale bars=100 μm).

3.4. Effect of Polymer Concentration on Honeycomb-like Structures

The structural and size-based investigation of honeycomb-like structures have been analysed when the PLGA-*b*-PEG concentration ranged between 2.5% and 10% (w/v). During the investigation water/oil phase flow rate was kept constant at 1 and monodispersed micro droplets were collected on glass slides. The average diameters were found to be decreasing with the increasing polymer concentration, nevertheless the change in size is not as remarkable as with flow rates as previously discussed. Table 3 summarizes the pore size investigation, with respect to PLGA-*b*-PEG concentration. The smallest pore diameter was measured as 124 μm at 10% (w/v) concentration of PLGA-*b*-PEG when DCM used as solvent. The same parameters resulted with 129 μm pores for the chloroform-based solution. The trend is also identical with 5% w/v PLGA-*b*-PEG concentration; however, 2.5% w/v solutions gives closer results for both solvents. At this point, relatively the large deviation in DCM solvent is remarkable and in addition to this, the distortion in porous pattern after bursting of perfectly aligned droplet structures is

noticed. The source of this irregularity was observed as the rapid bursting of micro droplets which was caused by several factors as discussed below. Although both DCM and chloroform has the same PLGA-*b*-PEG concentration, distorted patterns were only observed in DCM, which has lower viscosity with respect to chloroform i.e. viscosity value of PLGA-*b*-PEG (% 10 (w/v)) solution was found 13.2 mPa s for DCM and 24 mPa s for chloroform. As previously reported by Elsayed et al.[3], increasing the viscosity of the oil phase extend the life of the droplet surrounded by polymer, preventing chaotic pattern forming, which can be seen in the differences between the patterns in Figure 6a-c for DCM and d-f for chloroform. The pattern differences between two porous structures can also be related to the high vapour pressure of DCM. Micro droplets generated through the junction consists of aligned amphiphilic PLGA-*b*-PEG polymer chains, mainly deposited on the outer layer, as a result of interaction of PEG ends with dispersion phase, as previously discussed. At low concentrations, deposited amount of polymer in the outer region cannot stabilize the spherical form of structure because of the high vapour pressure, leading to a quicker rupture of droplet. However, honeycomb-like membranes with uniform spherical pores were obtained with chloroform, because of the relatively low vapour pressure than DCM ($CHCl_3$:160 mmHg and DCM:353 mmHg at 20 °C). Both high viscosity and low vapour pressure of chloroform had a combined effect on droplet bursting, resulting in a uniformity in size. Wall struts of honeycomb-like structures were also observed to be thicker and denser, compared to DCM samples.

Table 3. Effect of PLGA-*b*-PEG concentration on pore size of honeycomb-like structures.

		Concentration (w/v)		
	Solvent	2.5	5	10
Pore size (μm)	DCM	141±17	126±7	124±4
	Chloroform	142±7	131±8	129±6

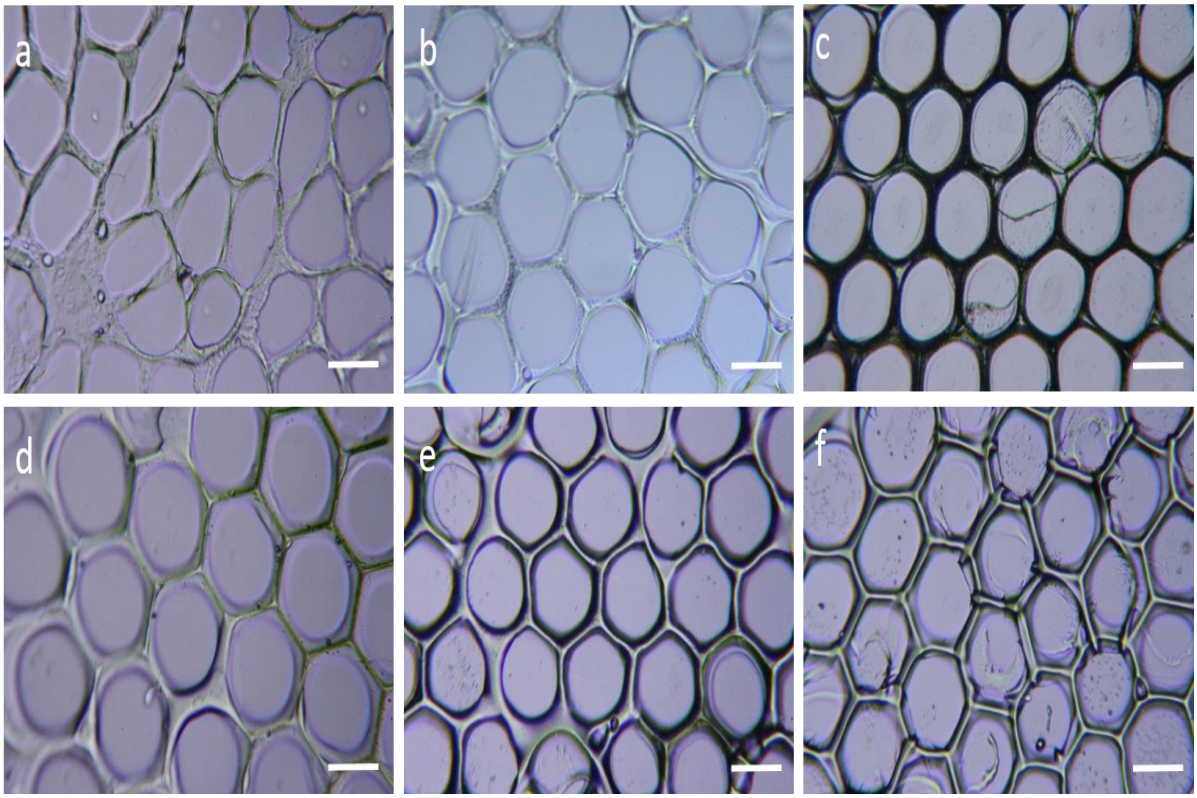

Figure 6. The effect of polymer concentration on honeycomb-like structure morphology in both DCM (a-c) and chloroform (d-f). PLGA-*b*-PEG concentrations are 2.5%, 5% and 10% by wt. from left to right, respectively. All scale bars indicate 100 μm.

3.5. Effect of Solvent on Nanoparticle Formation in the Honeycomb-like Structure

The effect of solvent type on honeycomb-like patterns was also investigated by a comparison between 5% PLGA-*b*-PEG solution (w/v) in both DCM and chloroform.

Although there were no major differences especially in size or morphology, as previously mentioned, tiny dark dots were noticed on honeycomb pattern struts in DCM (Figure 7d). During the high magnification SEM investigation, images of both samples were compared and spherical particles on DCM samples were noticed and further magnification of the area revealed that nanoparticles with size of 200-300 nanometres were embedded in the honeycomb strut walls. Breaking of fine droplets can give sub-micrometre size particles embedded in the structure after bursting[3]. However, in our case nanoparticles were spherical and had low polydispersity. The mechanism of nanoparticle generation from oil droplets can be explained by the Marangoni bursting phenomenon, recently proposed by Keiser et al. [32]. The outer side of the PLGA-*b*-PEG containing DCM droplet evaporates at a rapid rate at the water-oil interphase. At this interface diffusion is controlled, as the polymeric PLGA-*b*-PEG nanoparticles can only form and disperse in the direction of the evaporating solvent. Nanoparticle generation is sourced to the small daughter droplets breaking from the main droplet and the mini-emulsions generated by the Marangoni effect, which was caused by the surface tension difference between the centre and the outer region[33]. The surface tension at the interphase where the emulsion created is lower than the centre of the droplet so there is a continuous flow of polymer chains[34]. In this emulsion, daughter droplets disperse in the water phase and because of the amphiphilic nature of the PLGA-*b*-PEG, the orientation of chains are similar like surfactant structures, i.e. PEG blocks on the outer layer and longer PLGA chains entangled in the centre. Figure 7g shows the schematic representation of daughter droplet formation and precipitation. As the solvent completely evaporates from the daughter droplets, homogeneous polymeric nanoparticles are formed owing to precipitation. This nanoprecipitation and

instant forming phenomenon is addressed to interfacial interactions between two liquid phases[35]. The formed particles up to complete burst of microfluidic droplet did not merge to create secondary structures since the solvent concentration (DCM) is too low to dissolve.

In contrast, this result was not observed in the case with use of chloroform as solvent, as can be seen in SEM image (Figure 7b). This discrepancy can be explained by the solubility difference between two solvents. Although both chloroform and DCM are known to be immiscible in water phase, the solubility of DCM is more than two times bigger than chloroform at ambient temperature, which makes DCM much more favoured in conventional nanoparticle synthesis[36-37]. The Marangoni number (Ma) equation, which is defined as the proportion of thermal/surface tension forces divided by viscous forces is:

$$\mathrm{Ma} = -\frac{d\gamma}{dT}\frac{L\Delta T}{\eta\alpha} \qquad (3)$$

Where "γ" is surface tension, "L" is length, "α" is thermal diffusivity, "η" is dynamic viscosity and "ΔT" is temperature difference[38]. Equation 3 explains the Marangoni flow is affected by several parameters, especially by temperature gradient between the surface and core of the droplet and viscosity[39-40]. Since DCM has a lower boiling than chloroform the temperature at the outer layer is expected to be lower than that of chloroform, as the rest of the parameters are kept constant. Additionally, relatively high viscosity of chloroform compared to DCM with same concentration of PLGA-*b*-PEG, also decreases the Marangoni number, which reduces the Marangoni flow.

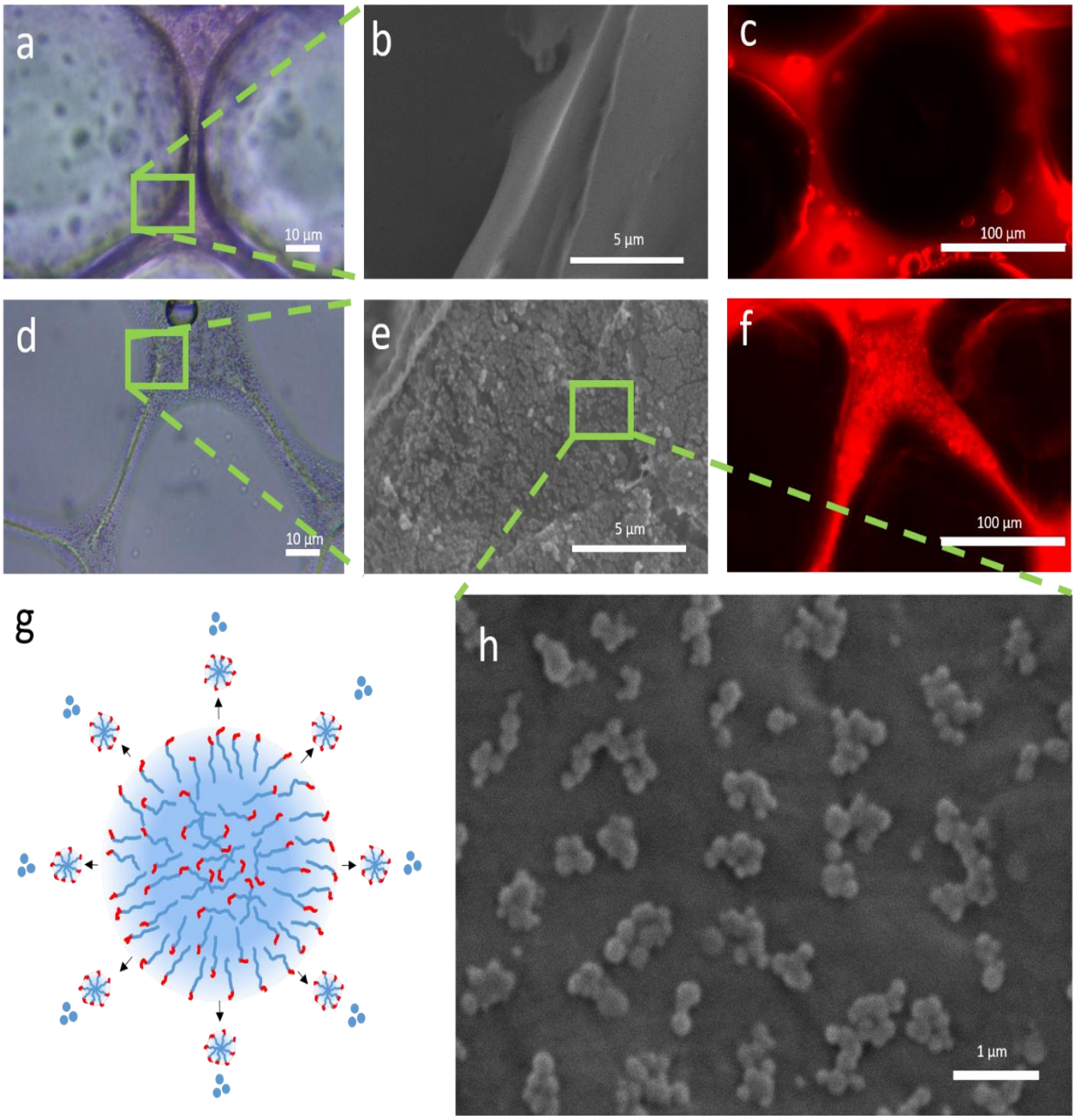

Figure 7. Solvent dependent nanoparticle formation on the PLGA-*b*-PEG honeycomb-like structure a)Optical microscope image of strut (scale bar=100µm), b)SEM image of strut (scale bar=5µm), c)Fluorescent microscope image of strut (scale bar=100µm) produced with chloroform as solvent, d)Optical microscope image of strut (scale bar=100µm), e)SEM image of strut (scale bar=5µm), f)Fluorescent microscope image of strut (scale bar=100µm) produced with DCM as solvent, g)Schematic representation of nanoparticle production via Marangoni bursting, h)SEM image of nanoparticles (scale bar=1µm) produced with DCM as solvent. Green boxes show nanoparticle absence (a) and presence (d and e).

4. CONCLUSIONS

PLGA-*b*-PEG is a widely used polymer in biomaterials, drug delivery and tissue engineering studies. In this study, PLGA-*b*-PEG porous structures with honeycomb-like surface pattern were obtained via highly monosized micro droplets generated by a T-junction microfluidics system. Micro droplets were collected on glass slides and porous structures were obtained after bursting of droplets. In addition to that, nanoparticles embedded struts were also noticed in some samples indicating that PLGA-*b*-PEG gathered at the edge of the droplet creating a ring structure and the break-up of this ring before complete bursting of the micrometre size droplet results in nanoparticle formation. T-junction processing of honeycomb-like surfaces has great potential and can be used in biomedical applications, especially in drug delivery related studies with nanoparticle forming ability and cellular responses to different surface morphologies.

Acknowledgements

This study was supported by Hacettepe University, Scientific Research Projects Coordination Unit Grant No: TDK-2017-14725 and Grant No: FBI-2017-14296.

LIST OF SUPPLEMENTARY INFORMATION (SI)

SI 1 T-junction movie

SI 2 Tip End Movie

GRAPHICAL ABSTRACT

Fluorescence microscope image of PLGA-*b*-PEG honeycomb-like structure formed using DCM solution.

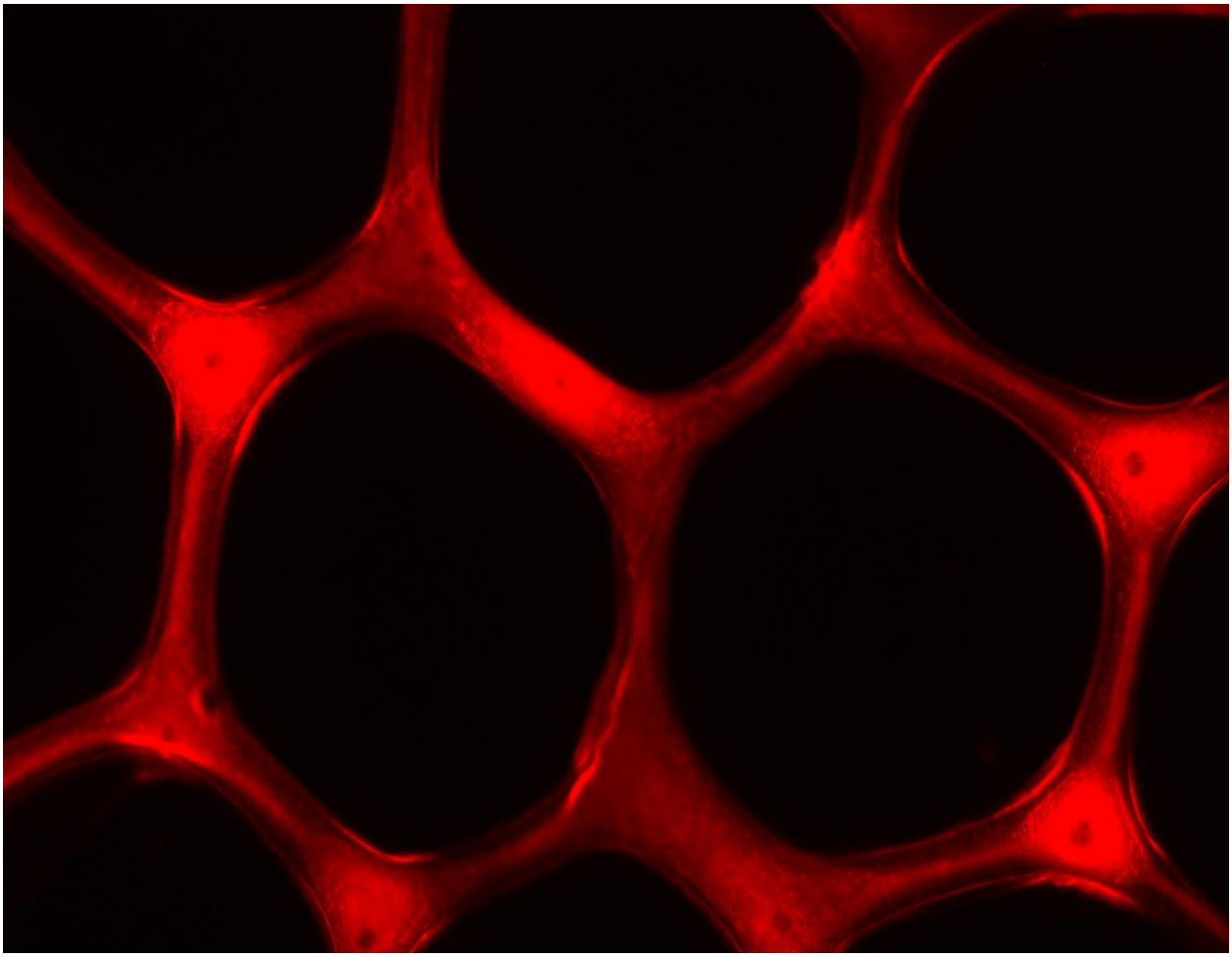

REFERENCES

1. Li, B.; Kan, L.; Zhang, X. Y.; Li, J.; Li, R. T.; Gui, Q. Y.; Qiu, D. L.; He, F.; Ma, N.; Wang, Y. P.; Wei, H., Biomimetic Bone-like Hydroxyapatite by Mineralization on Supramolecular Porous Fiber Networks. *Langmuir* **2017,** *33* (34), 8493-8502.
2. Zhou, W. D.; Chen, Y.; Roh, T.; Lin, Y. N.; Ling, S. J.; Zhao, S. W.; Lin, J. D.; Khalil, N.; Cairns, D. M.; Manousiouthakis, E.; Tse, M.; Kaplan, D. L., Multifunctional Bioreactor System for Human Intestine Tissues. *Acs Biomaterials Science & Engineering* **2018,** *4* (1), 231-239.

3. Elsayed, M.; Kothandaraman, A.; Edirisinghe, M.; Huang, J., Porous Polymeric Films from Microbubbles Generated Using a T-Junction Microfluidic Device. *Langmuir* **2016,** *32* (50), 13377-13385.
4. Wang, C. C.; Yang, K. C.; Lin, K. H.; Wu, C. C.; Liu, Y. L.; Lin, F. H.; Chen, I. H., A biomimetic honeycomb-like scaffold prepared by flow-focusing technology for cartilage regeneration. *Biotechnology and bioengineering* **2014,** *111* (11), 2338-2348.
5. Wang, C. C.; Yang, K. C.; Lin, K. H.; Liu, H. C.; Lin, F. H., A highly organized three-dimensional alginate scaffold for cartilage tissue engineering prepared by microfluidic technology. *Biomaterials* **2011,** *32* (29), 7118-26.
6. Çelik, E.; Bayram, C.; Akçapınar, R.; Türk, M.; Denkbaş, E. B., The effect of calcium chloride concentration on alginate/Fmoc-diphenylalanine hydrogel networks. *Materials Science and Engineering: C* **2016,** *66*, 221-229.
7. Karimpoor, M.; Illangakoon, E.; Reid, A. G.; Claudiani, S.; Edirisinghe, M.; Khorashad, J. S., Development of artificial bone marrow fibre scaffolds to study resistance to anti-leukaemia agents. *British journal of haematology* **2017**.
8. Karnik, R.; Gu, F.; Basto, P.; Cannizzaro, C.; Dean, L.; Kyei-Manu, W.; Langer, R.; Farokhzad, O. C., Microfluidic platform for controlled synthesis of polymeric nanoparticles. *Nano letters* **2008,** *8* (9), 2906-2912.
9. Rhee, M.; Valencia, P. M.; Rodriguez, M. I.; Langer, R.; Farokhzad, O. C.; Karnik, R., Synthesis of Size-Tunable Polymeric Nanoparticles Enabled by 3D Hydrodynamic Flow Focusing in Single-Layer Microchannels. *Advanced Materials* **2011,** *23* (12).
10. Ma, J.; Lee, S. M.-Y.; Yi, C.; Li, C.-W., Controllable synthesis of functional nanoparticles by microfluidic platforms for biomedical applications–a review. *Lab on a Chip* **2017,** *17* (2), 209-226.
11. Lorenceau, E.; Utada, A. S.; Link, D. R.; Cristobal, G.; Joanicot, M.; Weitz, D. A., Generation of Polymerosomes from Double-Emulsions. *Langmuir* **2005,** *21* (20), 9183-9186.
12. Utada, A. S.; Lorenceau, E.; Link, D. R.; Kaplan, P. D.; Stone, H. A.; Weitz, D. A., Monodisperse double emulsions generated from a microcapillary device. *Science (New York, N.Y.)* **2005,** *308* (5721), 537-41.
13. Wang, B.; Prinsen, P.; Wang, H.; Bai, Z.; Wang, H.; Luque, R.; Xuan, J., Macroporous materials: microfluidic fabrication, functionalization and applications. *Chem Soc Rev* **2017,** *46* (3), 855-914.
14. Carroll, N. J.; Rathod, S. B.; Derbins, E.; Mendez, S.; Weitz, D. A.; Petsev, D. N., Droplet-based microfluidics for emulsion and solvent evaporation synthesis of monodisperse mesoporous silica microspheres. *Langmuir* **2008,** *24* (3), 658-661.
15. Chung, K.-y.; Mishra, N. C.; Wang, C.-c.; Lin, F.-h.; Lin, K.-h., Fabricating scaffolds by microfluidics. *Biomicrofluidics* **2009,** *3* (2), 022403.
16. Colosi, C.; Costantini, M.; Barbetta, A.; Pecci, R.; Bedini, R.; Dentini, M., Morphological comparison of PVA scaffolds obtained by gas foaming and microfluidic foaming techniques. *Langmuir* **2013,** *29* (1), 82-91.
17. Liu, D.; Zhang, H.; Fontana, F.; Hirvonen, J. T.; Santos, H. A., Microfluidic-assisted fabrication of carriers for controlled drug delivery. *Lab on a Chip* **2017,** *17* (11), 1856-1883.
18. Baby, T.; Liu, Y.; Middelberg, A. P.; Zhao, C.-X., Fundamental studies on throughput capacities of hydrodynamic flow-focusing microfluidics for producing monodisperse polymer nanoparticles. *Chemical Engineering Science* **2017,** *169*, 128-139.

19. Engelmayr Jr, G. C.; Cheng, M.; Bettinger, C. J.; Borenstein, J. T.; Langer, R.; Freed, L. E., Accordion-like honeycombs for tissue engineering of cardiac anisotropy. *Nature materials* **2008,** *7* (12), 1003.
20. Eniwumide, J. O.; Tanaka, M.; Nagai, N.; Morita, Y.; De Bruijn, J.; Yamamoto, S.; Onodera, S.; Kondo, E.; Yasuda, K.; Shimomura, M., The morphology and functions of articular chondrocytes on a honeycomb-patterned surface. *BioMed research international* **2014,** *2014*.
21. Andrieux, S. b.; Drenckhan, W.; Stubenrauch, C., Generation of Solid Foams with Controlled Polydispersity Using Microfluidics. *Langmuir* **2018**.
22. Ding, S.; Attia, M. F.; Wallyn, J.; Taddei, C.; Serra, C. A.; Anton, N.; Kassem, M.; Schmutz, M.; Er-Rafik, M.; Messaddeq, N., Microfluidic-assisted production of size-controlled SPIONs-loaded PMMA nanohybrids. *Langmuir* **2018**.
23. Şimşek, S.; Eroğlu, H.; Kurum, B.; Ulubayram, K., Brain targeting of Atorvastatin loaded amphiphilic PLGA-b-PEG nanoparticles. *Journal of microencapsulation* **2013,** *30* (1), 10-20.
24. Sari, E.; Tunc-Sarisozen, Y.; Mutlu, H.; Shahbazi, R.; Ucar, G.; Ulubayram, K., ICAM-1 targeted catalase encapsulated PLGA-b-PEG nanoparticles against vascular oxidative stress. *Journal of microencapsulation* **2015,** *32* (7), 687-698.
25. Riley, T.; Stolnik, S.; Heald, C.; Xiong, C.; Garnett, M.; Illum, L.; Davis, S.; Purkiss, S.; Barlow, R.; Gellert, P., Physicochemical evaluation of nanoparticles assembled from Poly (lactic acid)− Poly (ethylene glycol)(PLA− PEG) block copolymers as drug delivery vehicles. *Langmuir* **2001,** *17* (11), 3168-3174.
26. De Menech, M.; Garstecki, P.; Jousse, F.; Stone, H., Transition from squeezing to dripping in a microfluidic T-shaped junction. *journal of fluid mechanics* **2008,** *595*, 141-161.
27. Baroud, C. N.; Gallaire, F.; Dangla, R., Dynamics of microfluidic droplets. *Lab on a Chip* **2010,** *10* (16), 2032-2045.
28. van Steijn, V.; Kleijn, C. R.; Kreutzer, M. T., Predictive model for the size of bubbles and droplets created in microfluidic T-junctions. *Lab on a Chip* **2010,** *10* (19), 2513-2518.
29. Xu, J.; Li, S.; Tan, J.; Luo, G., Correlations of droplet formation in T-junction microfluidic devices: from squeezing to dripping. *Microfluidics and Nanofluidics* **2008,** *5* (6), 711-717.
30. Nisisako, T.; Torii, T.; Higuchi, T., Droplet formation in a microchannel network. *Lab on a Chip* **2002,** *2* (1), 24-26.
31. Garstecki, P.; Fuerstman, M. J.; Stone, H. A.; Whitesides, G. M., Formation of droplets and bubbles in a microfluidic T-junction-scaling and mechanism of break-up. *Lab Chip* **2006,** *6* (3), 437-46.
32. Keiser, L.; Bense, H.; Colinet, P.; Bico, J.; Reyssat, E., Marangoni Bursting: Evaporation-Induced Emulsification of Binary Mixtures on a Liquid Layer. *Physical review letters* **2017,** *118* (7), 074504.
33. Kamperman, T.; Visser, C. W.; Karbaat, L.; Lohse, D.; Karperien, M., In-air Microfluidics Enables Rapid Fabrication of Emulsions, Suspensions, and 3D Modular (Bio) materials. *Microgel Technology To Advance Modular Tissue Engineering* **2018**, 121.
34. Kamaly, N.; Fredman, G.; Subramanian, M.; Gadde, S.; Pesic, A.; Cheung, L.; Fayad, Z. A.; Langer, R.; Tabas, I.; Cameron Farokhzad, O., Development and in vivo efficacy of targeted polymeric inflammation-resolving nanoparticles. *Proceedings of the National Academy of Sciences of the United States of America* **2013,** *110* (16), 6506-6511.
35. Luque-Alcaraz, A.; Lizardi-Mendoza, J.; Goycoolea, F.; Higuera-Ciapara, I.; Argüelles-Monal, W., Preparation of chitosan nanoparticles by nanoprecipitation and their ability as a drug nanocarrier. *RSC Advances* **2016,** *6* (64), 59250-59256.

36. Cheng, J.; Teply, B. A.; Sherifi, I.; Sung, J.; Luther, G.; Gu, F. X.; Levy-Nissenbaum, E.; Radovic-Moreno, A. F.; Langer, R.; Farokhzad, O. C., Formulation of functionalized PLGA–PEG nanoparticles for in vivo targeted drug delivery. *Biomaterials* **2007,** *28* (5), 869-876.
37. Baysal, I.; Ucar, G.; Gultekinoglu, M.; Ulubayram, K.; Yabanoglu-Ciftci, S., Donepezil loaded PLGA-b-PEG nanoparticles: their ability to induce destabilization of amyloid fibrils and to cross blood brain barrier in vitro. *Journal of Neural Transmission* **2017,** *124* (1), 33-45.
38. Guzman, R.; Vasquez, D. A., Surface tension driven flow on a thin reaction front. *The European Physical Journal Special Topics* **2016,** *225* (13-14), 2573-2580.
39. Rongy, L.; De Wit, A., Steady Marangoni flow traveling with chemical fronts. *The Journal of chemical physics* **2006,** *124* (16), 164705.
40. Majumder, M.; Rendall, C. S.; Eukel, J. A.; Wang, J. Y.; Behabtu, N.; Pint, C. L.; Liu, T.-Y.; Orbaek, A. W.; Mirri, F.; Nam, J., Overcoming the "coffee-stain" effect by compositional Marangoni-flow-assisted drop-drying. *The Journal of Physical Chemistry B* **2012,** *116* (22), 6536-6542.